Article

PM$_{2.5}$ Estimation and Spatial-Temporal Pattern Analysis Based on the Modified Support Vector Regression Model and the 1 km Resolution MAIAC AOD in Hubei, China

Nengcheng Chen [1,2], Meijuan Yang [1], Wenying Du [1,*] and Min Huang [1]

1 State Key Laboratory for Information Engineering in Surveying, Mapping and Remote Sensing (LIESMARS), Wuhan University, Wuhan 430072, China; cnc@whu.edu.cn (N.C.); yang.m.j@whu.edu.cn (M.Y.); minhuang@whu.edu.cn (M.H.)
2 Collaborative Innovation Centre of Geospatial Technology, Wuhan University, Wuhan 430079, China
* Correspondence: duwenying@whu.edu.cn

Abstract: The satellite-retrieved Aerosol Optical Depth (AOD) is widely used to estimate the concentrations and analyze the spatiotemporal pattern of Particulate Matter that is less than or equal to 2.5 microns (PM$_{2.5}$), also providing a way for the related research of air pollution. Many studies generated PM$_{2.5}$ concentration networks with resolutions of 3 km or 10 km. However, the relatively coarse resolution of the satellite AOD products make it difficult to determine the fine-scale characteristics of PM$_{2.5}$ distributions that are important for urban air quality analysis. In addition, the composition and chemical properties of PM$_{2.5}$ are relatively complex and might be affected by many factors, such as meteorological and land cover type factors. In this paper, an AOD product with a 1 km spatial resolution derived from the Multi-Angle Implementation of Atmospheric Correction (MAIAC) algorithm, the PM$_{2.5}$ measurements from ground sites and the meteorological data as the auxiliary variable, are integrated into the Modified Support Vector Regression (MSVR) model that proposed in this paper to estimate the PM$_{2.5}$ concentrations and analyze the spatiotemporal pattern of PM$_{2.5}$. Considering the relatively small dataset and the somewhat complex relationship between the variables, we propose a Modified Support Vector Regression (MSVR) model that based on SVR to fit and estimate the PM$_{2.5}$ concentrations in Hubei province of China. In this paper, we obtained Cross Correlation Coefficient (R^2) of 0.74 for the regression of independent and dependent variables, and the conventional SVR model obtained R^2 of 0.60 as comparison. We think our MSVR model obtained relatively good performance in spite of many complex factors that might impact the accuracy. We then utilized the optimal MSVR model to perform the PM$_{2.5}$ estimating, analyze their spatiotemporal patterns, and try to explain the possible reasons for these patterns. The results showed that the PM$_{2.5}$ estimations retrieved from 1 km MAIAC AOD could reflect more detailed spatial distribution characteristics of PM$_{2.5}$ and have higher accuracy than that from 3 km MODIS AOD. Therefore, the proposed MSVR model can be a better method for PM$_{2.5}$ estimating, especially when the dataset is relatively small.

Keywords: PM$_{2.5}$; MAIAC 1 km AOD; MODIS; modified support vector regression; meteorological data

1. Introduction

Currently, air pollution and its related health problems have become research hot spots [1]. Numerous studies have indicated that particles smaller than 2.5 μm in aerodynamic diameter (PM$_{2.5}$) have adverse effects on human health and can cause pulmonary and cardiovascular diseases [2,3].

People exposed to polluted environments are prone to illness or even death. Thus, PM$_{2.5}$ exposure monitoring and pattern analysis are critical to air quality assessment and environmental epidemiologic studies [4,5]. PM$_{2.5}$ concentrations are traditionally obtained

by ground monitoring sites distributed throughout a country. However, the existing ground monitoring sites are too sparse to provide continuous $PM_{2.5}$ monitoring due to the high construction cost. In contrast, satellite remote sensing has wide and continuous spatial coverage and has been widely applied in the estimation of $PM_{2.5}$ concentrations [6,7], although the cloud could affect the availability of data.

Satellite-derived Aerosol Optical Depth (AOD) represents the quantity of light removed from a beam by the role of aerosol scattering or absorption during its path [8,9]. Furthermore, previous studies have indicated that there exists a direct relationship between the atmospheric particles (such as $PM_{2.5}$) and AOD [10]. Thus, remote sensing satellites' AOD products provide a potentially cost-effective way to estimate ground-level $PM_{2.5}$ mass concentrations [11,12]. A series of AOD products have been applied to such surveys [13], e.g., the Moderate Resolution Imaging Spectroradiometer (MODIS) [14,15], the Multi-angle Imaging Spectroradiometer [16], the Himawari-8 (H8) [17,18], and the Visible Infrared Imaging Radiometer Suite [19]. However, the relatively coarse spatial resolutions (usually 3 km or 10 km) of the above-mentioned satellite sensors limit the precise estimates of $PM_{2.5}$ in urban areas. Recently, the Multi-Angle Implementation of Atmospheric Correction (MA-IAC) algorithm, which utilizes time-series analysis and image-based processing techniques, was developed to conduct aerosol retrievals and atmospheric corrections.

The Multiangle Implementation of Atmospheric Correction (MAIAC) is a new generic algorithm applied to collection 6 (C6) MODIS measurements to retrieve Aerosol Optical Depth (AOD) over land at high spatial resolution (1 km) [20]. The related AOD product MCD19A2 (MODIS Collection 6 (C6) daily AOD dataset), which is based on the MAIAC algorithm, was released in 2018 [21]. Although the goal of the MAIAC AOD product is aerosol monitoring, this product of 1 km resolution gives us chance to estimate $PM_{2.5}$ concentrations in a higher spatial and temporal resolution.

Previous studies have shown that the relationship between $PM_{2.5}$ and AOD is relatively complex and may be affected by a series of parameters, such as the aerosol type and the vertical structure of aerosol distribution [22], the relative humidity (RH) [23], planetary boundary layer height (PBLH) [24], wind speed and direction [25], the depth and temperature difference of the inversion layer [24], land cover [26], etc. Furthermore, recently, more sophisticated methods used to estimate $PM_{2.5}$ have been developed by taking into account these parameters.

Studies have tried to explore the relationship between these variables by statistical approaches. There have been many different approaches proposed by studies that explored the relationship between $PM_{2.5}$ and AOD. For example, including but not limited to, the linear regression model, the geographically weighted regression model [27,28], the two-stage model [29] and the newly developed neural network methods [30,31]. As geospatial data, $PM_{2.5}$ concentration data have spatial heterogeneity and spatial dependence. The statistical characteristics of $PM_{2.5}$ concentrations may vary over space and time. This space–time anisotropy may violate the independent and identically distributed random variables in most of the machine learning methods [32].

The Support Vector Machine (SVM) based on the principle of structural risk minimization initially developed for solving classification problems using small sample learning is found to be promising for solving regression problems. The SVM for regression termed as Support Vector Regression (SVR) has revealed superior performance due to its inherent capability to circumvent overfitting problem in regression and improved response approximation ability [33].

Considering the characteristics of the experiment:

1. Nonlinear and complex relationship; as an atmospheric research, the relationship between $PM_{2.5}$, AOD and auxiliary variables is rather complicated and it would be better to describe it with nonlinear model. The kernel function can simplify the inner product operation in the mapping space, avoiding calculating in the high-dimensional space directly.

2. The relatively small dataset. Regression algorithms generally obey the law of big data; this means that the final result is relatively more accurate with more samples. The SVM makes it possible to achieve relatively good results on small samples. SVR based on the support vector machine solves regression problems using small sample learning. Furthermore, the 'small sample' is a considerable concept; we think the samples in our experiment are enough for digging out the nonlinear relationship.

3. The capability to handle high-dimensional data sets well. SVR can grasp the nonlinear relationship between data and features on relatively small datasets, especially compared to most other machine learning methods.

Thus, this paper proposes the modified SVR (MSVR) method to improve the estimation accuracy of $PM_{2.5}$ concentrations. MSVR considers the impacts of spatial distance on estimation accuracy and adds factors in the model input that are generally included and contribute relatively more significant influence, with MAIAC AOD as the primary predictor and the meteorological and land cover information as ancillary information.

2. Materials and Methodology

2.1. Study Area

The study area of this paper is Hubei, China. Hubei Province is located in central China, and its capital city, Wuhan, is one of the largest cities and developing centers of the country (Figure 1). With the rapid development of urbanization and industrialization in China, climate disasters, such as smog, frequently occur in large cities in China as a result of worsening atmospheric and environmental conditions [34]. Research on $PM_{2.5}$ estimation and analysis in Wuhan can provide constructive guidance for urban air quality research in other large cities in China. Meanwhile, due to the complex climate and land cover of Hubei Province, research in this area can help analyze the effects of various factors such as climate and land cover on $PM_{2.5}$ distribution.
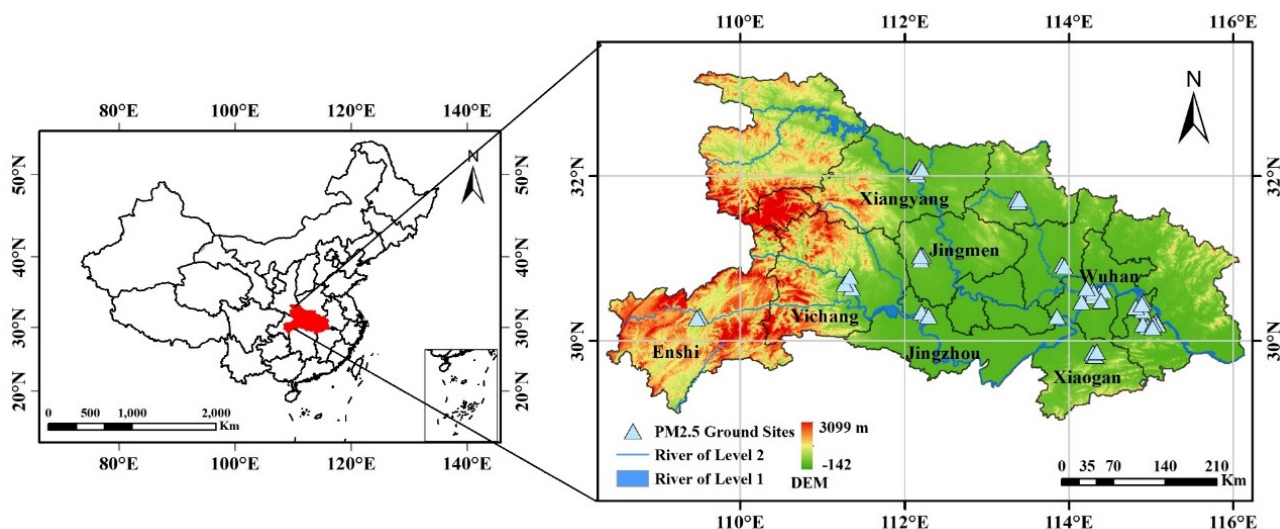

Figure 1. The study area and the monitoring sites were distributed in Hubei Province, and the total number of monitoring sites was 47 at 2017.

2.2. Experimental Data

2.2.1. MAIAC and MODIS AOD Data

The MAIAC algorithm is an advanced algorithm for aerosol retrievals and atmospheric correction for MODIS data over both dark vegetated and bright desert surfaces. This algorithm explores the advantages of time-series processing at a synergistic level for cloud masking and aerosol-surface retrievals. The MAIAC algorithm uses up to 16 days of gridded MODIS measurements to make simultaneous retrievals of AOD and surface bidirectional reflectance distribution factor (BRF)/albedo and then produces the AOD at

a 1 km resolution. The algorithm uses both individual grid cells (also called pixels) and fixed-size (25×25 km^2) areas (also called blocks), as required by the cloud mask algorithm and retrieval [21].

Studies have indicated that MAIAC AOD agreed well with AERONET AOD (Aerosol Robotic Network AOD), which is commonly considered as the ground true values of AOD [35]. Additionally, comparison studies between the satellite AOD and the AERONET AOD showed that the MAIAC algorithm improved the accuracy than MODIS DB (Deep Blue)/DT (Dark Target) [36]. Mhawish [20] obtained RMSE 0.148 for MAIAC, 0.198 for MODIS DB, and 0.183 for MODIS DT.

AERONET AOD currently has 61 stations distributed in China, but there are no stations in our research area, Hubei Province. Therefore, we may not be able to conduct a comparison of AERONET and MODIS data in the study area of the study period. Furthermore, there has been research that gained the insights regarding the performance of MAIAC algorithm by comparing MAIAC aerosol products with the ground-based observations at nine typical sites spread out in China. The research indicated that MAIAC and ground-observed AOD values showed high correlation coefficient (R of most sites reached higher than 0.85 or even 0.9) in spite of the complicated surface types, diverse aerosol sources, and heavy loading of aerosols in the vast atmosphere of China. MODIS MAIAC 1 km AOD at 550 nm, compared with AERONET measurements in Xuzhou and Taihu sites that are relatively close to our research area, obtained R of 0.91 and 0.878. More and more studies have applied MAIAC AOD to PM$_{2.5}$ inversion in China. We believe that this AOD product has quality assurance over China.

2.2.2. Auxiliary Variables

Because atmospheric flow is affected by meteorological parameters (e.g., temperature and humidity) [25] and because air pollutants may be absorbed by some land cover types (e.g., vegetation) [37], meteorological parameters and land cover parameters were adopted as auxiliary variables in our algorithm to improve the estimation accuracy of PM$_{2.5}$.

- Meteorological data

Boundary layer height (BLH, m) refers to the thickness of the planet's boundary layer and is one of the important physical parameters for atmospheric numerical model and atmospheric environment evaluation. Usually, BLH has a negative relationship with PM$_{2.5}$ because a higher BLH can expand the near-surface atmosphere and facilitate vertical convection. Humidity can influence the concentration of PM$_{2.5}$ by changing the weight of particulates and further affecting the diffusion speed of pollutants [38]. Temperature has a negative relationship with PM$_{2.5}$ because the inversion layer caused by low temperature is not conducive to the convection of the atmosphere [39]. Therefore, in this paper, the three types of meteorological parameters, BLH, relative humidity (RH, %), and 2 m near-ground-temperature (T, °C), were adopted in our algorithm to improve the estimation accuracy.

The BLH, RH, and T data employed in this paper were obtained from the European Centre for Medium-Range Weather Forecasts (ECMWF) (https://www.ecmwf.int/). The ECMWF provides quality controlled spatially and temporally consistent, real-time, current forecasts, climate reanalysis and specific datasets. The data assimilation system used to produce ERA-Interim was based on a 2006 release of the IFS (Cy31r2). The system includes a 4-dimensional variation analysis (4D-Var) with a 12-h analysis window. The spatial resolution of the data set is approximately 80 km (T255 spectral) on 60 vertical levels, from the surface up to 0.1 hPa, and at a horizontal resolution of 0.125° × 0.125°, and its temporal resolution is 3 h.

- Land cover data

Land cover variables, especially vegetation coverage and construction parameters, can influence the performance of the AOD-PM$_{2.5}$ regression models [40]. Studies have shown that vegetation coverage has an obvious effect on reducing and redistributing atmospheric particulate matters by means of sedimentation, retardation and adsorptions. It is worth

noting that these effects will change with the change of seasons, because some vegetation will have different states in different seasons. Generally, winter vegetation has the smallest reduction effect on $PM_{2.5}$ [41]. Conversely, construction land produces dust and other pollutants that increase the concentration of atmospheric pollutants.

Land cover data with a 1 km spatial resolution were utilized in this paper. The data were obtained from the "Remote sensing monitoring data of land cover in China" section on the website of the Chinese Academy of Sciences Data Centre for Resources and Environmental Sciences (http://www.resdc.cn). It provides a database of multi-phase land cover status for the national land area under the years of accumulation generated by manual visual interpretation and based on the Landsat TM/ETM remote sensing image data. The land cover types include six primary types: cultivated land, forestland, grassland, waters, residential areas and unused land.

2.2.3. Ground $PM_{2.5}$ Measurements

The ground $PM_{2.5}$ measurements were used as training data and testing data in our algorithm to obtain the relationship between $PM_{2.5}$ and AOD and were then utilized to generate continuous $PM_{2.5}$. As shown in Figure 1, there are 47 national ground monitoring sites in the study area (Hubei Province). The 47 sites are mainly located in densely populated cities, such as Wuhan (10 sites), and there are rural areas without ground sites. The $PM_{2.5}$ measurements in four seasons of 2017 from these sites were used in the experiment of this paper. The $PM_{2.5}$ hourly data were collected from the PM25.IN website (http://www.pm25.in/) provided by the China National Environmental Monitoring Center (CNEMC); as for worldwide research, the $PM_{2.5}$ data can be obtained from the following website (http://www.aqicn.info/here/).

Terra and Aqua satellites passed over the equator at approximately 10:30 a.m. and 13:30 p.m. local time [42]. To ensure the time consistency of AOD and $PM_{2.5}$, we took the average of the hourly $PM_{2.5}$ measurements from 10:00 AM to 14:00 PM.

2.2.4. Data Pre-Processing and Integration

All the data and the descriptions were listed in Table 1.

Table 1. List of the data and variables adopted in the experiment.

Variables	Unit	Description	Temporal Period
$PM_{2.5}$	μg/m³	Particulate matter smaller than 2.5 μm in aerodynamic diameter	Hourly average of 10:00 am to 13:00 pm
AOD		Satellite-retrieved Aerosol Optical Depth	Daily data
RH	%	Relative Humidity	Hourly instantaneous data
BLH	(m)	Boundary Layer Height	
T	°C	2 m Temperature	
Land Cover		Vegetation coverage and construction factors	Remote sensing monitoring data of China's land use status in 2015

Four types of data were used in MSVR, including AOD, meteorological factors, land cover, and ground $PM_{2.5}$, and data pre-processing and integration were required due to the differences in the spatial coverage and observation frequency of the data. To ensure the spatial consistency of the data from multiple sources, all data were first re-projected to a unified coordinate system: The World Geodetic System 1984 geographic coordinate system [43,44].

On the one hand, the atmosphere is moving and circulating, thus the concentration of atmospheric particles at a certain location changes over time. On the other hand, variables in this research are not instantaneous data, but the average over a certain period of time. Therefore, we took the weighted average of 3×3 pixels centered on the grid.

Meanwhile, the forest and construction land-use data that significantly affected the formation and concentration of $PM_{2.5}$ were extracted with a buffer of 1 km from the ground monitoring sites. In terms of temporal consistency, the meteorological data were integrated to the average of the period from 10:00 AM to 14:00 PM local time to correspond to the period when Terra and Aqua passed over the equator. The extraction and integration of multi-source data were mainly implemented by coding in Python.

2.2.5. Model Constructing and Training

For better performance of MSVR, the datasets including all variables were first normalized to [0, 1]. As for the parameter setting of the MSVR model, we selected the RBF kernel for the kernel function considering the complicated relationships between all the variables. We listed a series of value combinations of the parameters "gamma" and "C" (penalty parameter) and then chose the optimal parameter values by grid searching.

Five-fold cross validation was employed in this experiment. The training dataset was first randomly split into five subsets, with approximately 20% of the total data record in each subset. In each round of cross-validation, one subset was selected to be used as validation samples, and the remaining subsets were utilized to train and fit the model.

In this experiment, three statistical indicators, including the R^2, the mean percentage error (MPE) and the square root of the mean squared prediction errors (RMSE), were calculated to assess the model performance. The accuracy evaluation and the comparison of the different models are discussed later in Section 4.1.

2.3. Principle of SVR

A Support Vector Machine (SVM) is a kind of machine learning method based on statistical learning theory, dimension theory and structural risk minimization principle. It shows many unique advantages in solving small sample, nonlinear and high-dimensional pattern recognition problems, and to a large extent overcomes the problems of "dimension disaster" and "over-learning" [45]. SVM is widely used to solve problems such as classification and nonlinear mapping and performs better in solving the problem of small sample datasets. SVM can, to a certain extent, solve the problems of model selection and over-learning that may be difficult for some traditional networks to solve.

Support Vector Regression (SVR) is the application of SVM in regression analysis [46], and it solves the regression task by transforming an inseparable problem of low-dimensional space into a linearly separable problem of high-dimensional space using the space mapping function [47]. We must find a hyperplane to fit the distribution of the sample data, which means minimizing the sum of the distance between the sample points and the hyperplane [48,49].

In this experiment, for a given set of training data, the variables x, y are both vectors. $\{(x_1, y_1), (x_2, y_2), \cdots, (x_i, y_i)\}$, $x \subset \mathbf{R}^n$ *and* $y \subset \mathbf{R}$, the problem of regression is to find the flattest function f that map a point in the space $\mathbf{R}^n$ onto the space $\mathbf{R}$ with the lowest expected risk.

The key of nonlinear SVR is to map the input vector $X \in \mathbf{R}^n$ into a high dimensional feature space $H \in R^m$ (with m larger than n), through mapping and then to solve a linear regression in space H.

$$\varphi(X) : X \to H \tag{1}$$

We call $\varphi(X)$ the mapping function, and usually the mapping function is difficult to calculate. Therefore, the kernel function $K(x, y)$ is introduced into SVR, where $\langle \varnothing(x), \varnothing(y) \rangle$ stands for the scalar product mapped to the feature space.

$$K(x, y) = \langle \varnothing(x), \varnothing(y) \rangle \tag{2}$$

In the high dimensional space, we can find a hyperplane to divide the sample points and the hyperplane is defined as below. ω is the normal vector, which determines the

direction of the hyperplane; b is the displacement, which determines the distance between the hyperplane and the origin.

$$\omega\phi(x) + b = 0 \tag{3}$$

The loss function of SVR was defined as

$$
L(f(x), y, \varepsilon) \\
= \begin{cases} 0, & |y - f(x)| \leq \varepsilon \\ |y - f(x)| - \varepsilon, & |y - f(x)| > \varepsilon \end{cases} \tag{4}
$$

where y is the true value corresponding to the dependent variable in the sample, $f(x)$ is the predicted value returned by the trained model, and ε describes the variation between the above y and $f(x)$.

The slack variables ξ_i, ξ_i^* are introduced, and then the initial nonlinear problem is converted to find the optimal values for ω and b, the parameters of the linear regression function. Thus, the solving process could be represented as the mathematical model below.

$$
\begin{cases}
min\frac{1}{2}||\omega||^2 + C\sum_{i=1}^{n}\left(\xi_i + \xi_i^*\right) \\
s.t. \begin{cases}
y_i - \omega\phi(x_i) - b \leq \varepsilon + \xi_i^* \\
-y_i + \omega\phi(x_i) + b \leq \varepsilon + \xi_i^*, \ i = 1, 2, \cdots, n \\
\xi_i \geq 0, \ \xi_i^* \geq 0
\end{cases}
\end{cases} \tag{5}
$$

2.4. Basi Idea of MSVR

A number of studies have indicated that the spatial distribution of $PM_{2.5}$ concentrations is distinct. According to the first law of geography, the farther the pixel is from the center pixel, the smaller the impact is [50]. However, the traditional SVR model utilized the general average method, and the different impacts of the pixel distances from the central value were ignored in the estimations of $PM_{2.5}$. $PM_{2.5}$ is most essentially characterized by its spatial and temporal heterogeneity, and many models such as the GWR and the GTWR models were proposed to cover these characteristics [33,51].

In this research, the SVR is modified and improved not only in making use of rich information of the input variables, but also in terms of extracting geospatial information weighted by the distance of adjacent pixels from a center pixel and the time difference from ground-based $PM_{2.5}$ measurements. Thus, the Modified SVR can also be called Space–Time Support Vector Regression. The basic structure of MSVR was clarified in Figure 2.
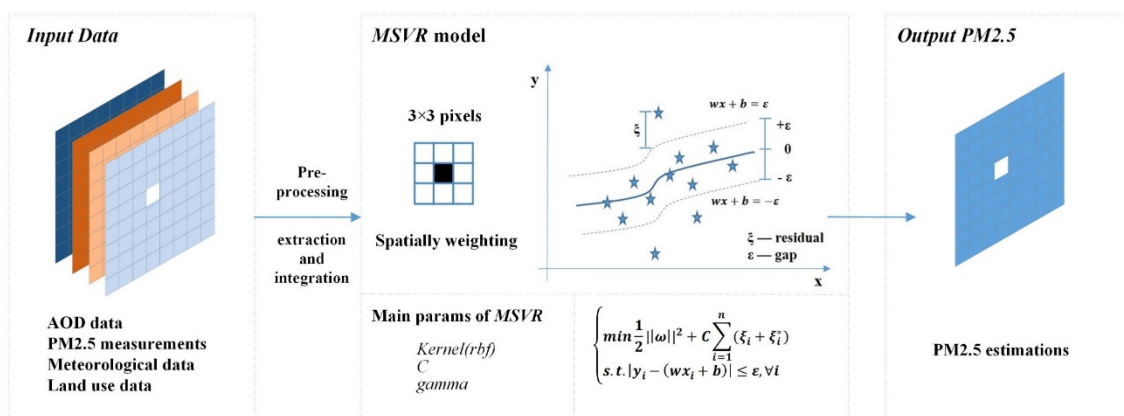

Figure 2. The main structure of the MSVR model.

For a given pixel, its spatial (Ps) and temporal (Pt) characteristics can be expressed as below,

$$\text{Ps} = \frac{\sum_{w=1}^{w} \frac{1}{ds_w^2} Ps_w}{\sum_{w=1}^{w} \frac{1}{ds_w^2}} \tag{6}$$

$$\text{Pt} = \frac{\sum_{l=1}^{L} \frac{1}{dt_l^2} Pt_l}{\sum_{l=1}^{L} \frac{1}{dt_l^2}} \tag{7}$$

where *ds* and *dt* represent the spatial and temporal distances. *W* and *L* represent the *w* pixels near the site and the *l* prior days for the same pixel.

When considering the spatial and temporal information, the model can be described as $\text{PM}_{2.5} = f$ (AOD, RH, BLH, T, LC, Ps, Pt).

In order to evaluate the accuracy of the model, we introduced commonly used regression evaluation indicators: R^2, MPE and RMSE. The specific meaning and calculation methods of these indicators are described as follows:

Cross correlation coefficient (also R^2) statistically quantifies the predictive accuracy of a statistical model. It shows the proportion of variance in the outcome variable that is explained by the predictions. It is also known as the cross correlation coefficient.

$$\mathbf{R}^2 = 1 - \frac{\sum_{i=1}^{n}(y_i - \hat{y}_i)^2}{\sum_{i=1}^{n}(y_i - \overline{y})^2} \tag{8}$$

Mean percentage error (MPE) that are reported in some statistical procedures are signed measures of error which indicate whether the forecasts are biased.

$$\mathbf{MPE} = \frac{100\%}{n} \sum_{i=1}^{n} \left| \frac{y_i - \hat{y}_i}{y_i} \right| \tag{9}$$

The root mean squared error (RMSE) is the square root of the mean squared error.

$$\mathbf{RMSE} = \sqrt{\frac{1}{n} \sum_{i=1}^{n}(y_i - \hat{y}_i)^2} \tag{10}$$

where y_i represents the true value, $\hat{y}_i$ represents the predicting value, $\overline{y}$ represents the average of all the true values.

3. Experiments and Results

3.1. MSVR Model Construction and PM$_{2.5}$ Estimations

3.1.1. Statistical Features of the Variables

To obtain an overview of the general situation and trend of the variables, the descriptive statistics of the variables used in the MSVR model are illustrated in Tables 2 and 3, including the mean, maximum (Max), minimum (Min), and standard deviation (Std. Dev.) for all the variables presented in the table. According to the table records, the 2017 annual mean $\text{PM}_{2.5}$ concentration for all monitoring sites in Hubei Province was 66.79 μg/m^3, and the maximum $\text{PM}_{2.5}$ concentration reached 344.66 μg/m^3, which was far beyond the standard of the World Health Organization Air Quality Interim Target of 35 μg/m^3 (WHO, 2006) and exceeded the allowable value (75 μg/m^3) of the Chinese air quality standard. These statistical data further demonstrate the great necessity of conducting $\text{PM}_{2.5}$ research and the rationality of selecting Hubei, China, as an experimental area.

Table 2. The descriptive statistics of the variables of 2017.

Variables	Mean	Max	Min	Std.Dev.
PM$_{2.5}$ (µg/m^3)	66.79	344.66	4.00	43.40
AOD (unit less)	0.48	3.27	0.09	0.31
Relative humidity (%)	3.5	13.8	0.6	4.7
BLH (km)	1.35	2.01	0.79	0.43
2m temperature (°C)	14.25	33.23	4.06	5.52

Table 3. The descriptive statistics of the variables of 2018.

Variables	Mean	Max	Min	Std.Dev.
PM$_{2.5}$ (µg/m^3)	52.91	328.00	2.33	34.70
AOD (unit less)	0.43	3.57	0.00	0.36
Relative humidity (%)	3.8	14.2	0.8	4.5
BLH (km)	1.41	2.86	0.84	0.58
2m temperature (°C)	14.73	36.44	2.36	6.89

3.1.2. Estimated PM$_{2.5}$ by MSVR

Before estimating the PM$_{2.5}$ based on the constructed MSVR method, we explored the relationships between PM$_{2.5}$ and AOD. The results demonstrated that the AOD had a positive relationship with the PM$_{2.5}$ concentrations, and when the site location or observation time changed, the AOD values and PM$_{2.5}$ concentrations had similar fluctuating trends. By utilizing the optimal MSVR model produced in the training process, we obtained continuous PM$_{2.5}$ estimations at a spatial resolution of 1 km. For visualization, we created a rendering map reflecting the concentration and distribution of PM$_{2.5}$ in the study area, which is shown in Figure 3. As shown in the graph, the PM$_{2.5}$ estimations had different values and distributions in different regions, and we discuss the details of these features in the following section.
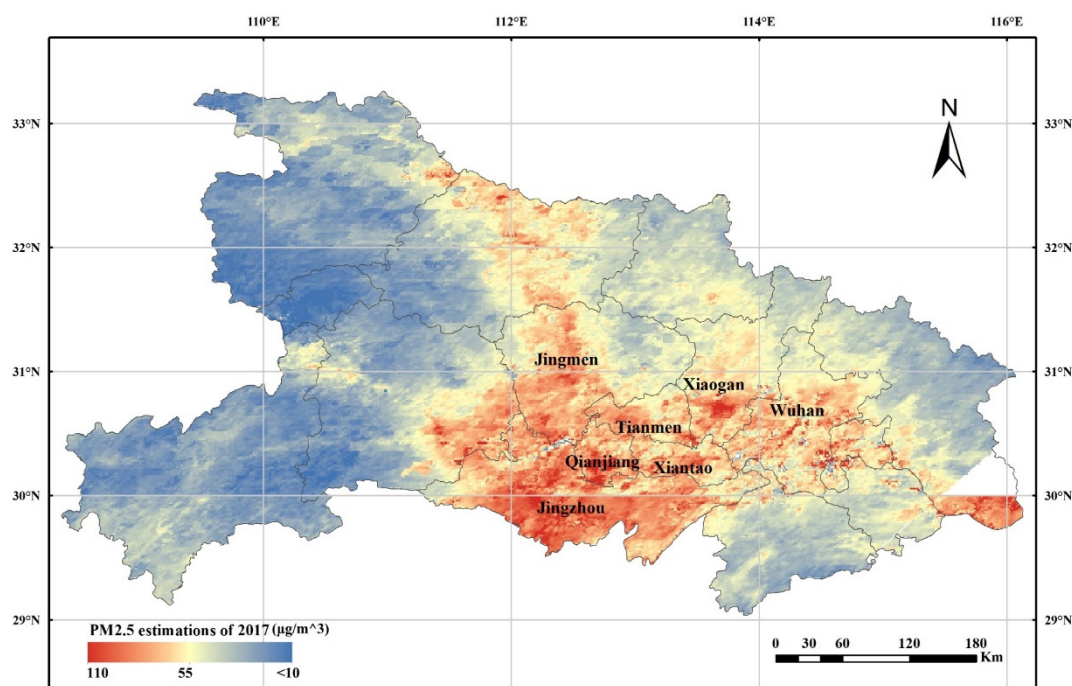

Figure 3. The estimated PM$_{2.5}$ average concentrations in the study area in 2017, with the selected optimal MSVR model at spatial resolutions of 1 km.

3.2. Pattern Analysis of PM$_{2.5}$ Concentrations

3.2.1. Spatial Pattern of the Estimated PM$_{2.5}$

The MSVR model proposed in this paper was used to estimate the continuous PM$_{2.5}$ concentrations in the study area at the grid resolutions of both 1 × 1 km from the MAIAC AOD and 3 × 3 km from the MODIS AOD. Although derived from different data sources, the distribution patterns of MAIAC- and MODIS-derived PM$_{2.5}$ were very similar, e.g., similar high-value areas and similar spatial variation patterns.

Whether from MAIAC or MODIS, the high PM$_{2.5}$ concentrations generally occurred in developed urban cities where the population and pollution sources were concentrated, while the low PM$_{2.5}$ concentrations usually occurred in rural areas or mountainous areas as it was demonstrated in the literature. In the study area of Hubei Province, the high values were mainly distributed in Wuhan, Xiangyang, Jingzhou and other quickly developing cities.

As shown in Figure 4, although the PM$_{2.5}$ of MODIS and MAIAC have extremely similar spatial distributions in 2017, the 1 km PM$_{2.5}$ from MAIAC has indisputable advantages in terms of resolution. When the study area was zoomed out to a smaller scale, such as an urban area, the 3 km PM$_{2.5}$ could describe only the general spatial variation, and the pixels became relatively coarse and difficult to read. However, the 1 km PM$_{2.5}$ derived from MAIAC AOD were able to reflect subtler spatial changes and could distinguish the pixels with high levels of PM$_{2.5}$ from the others; this difference enabled us to locate the pollution sources.
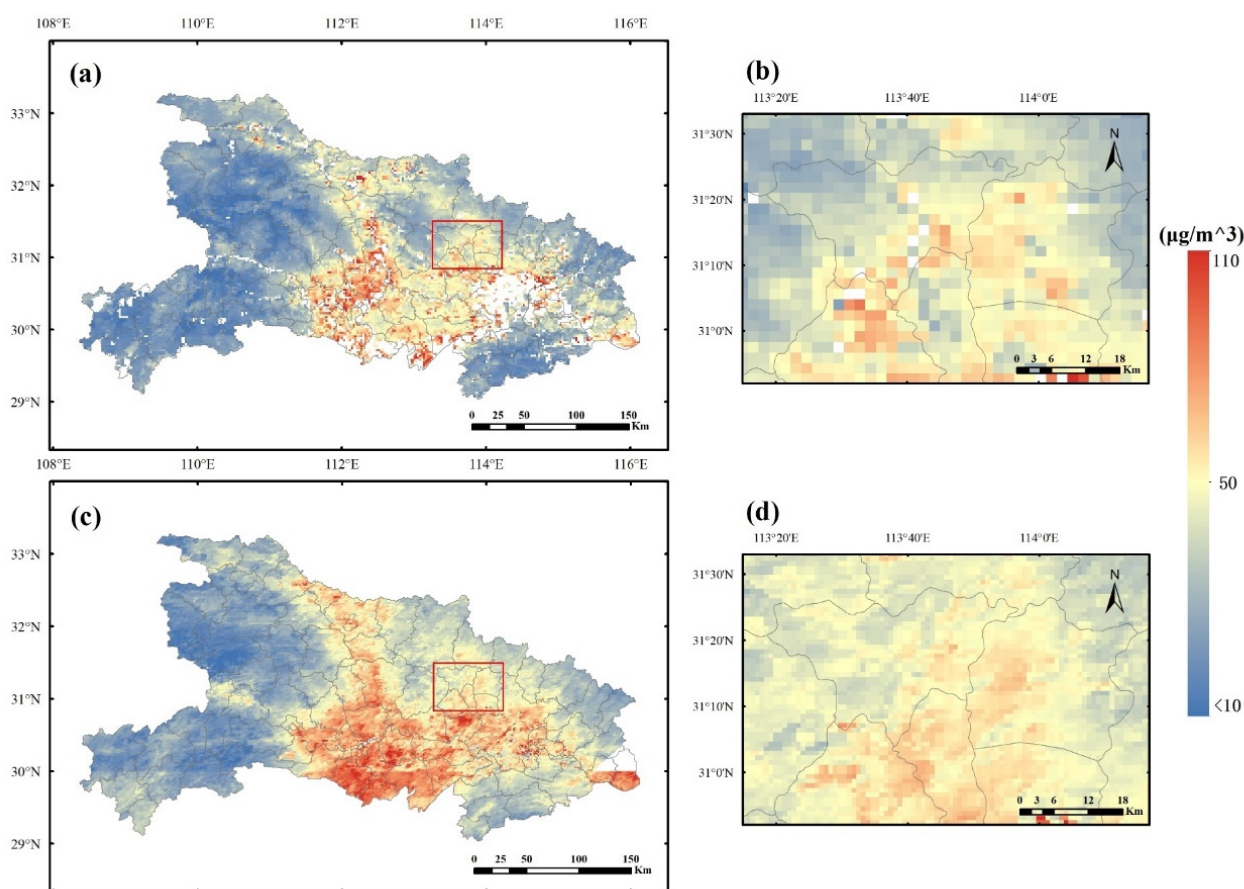

Figure 4. Spatial resolution comparison of the annual 1 km PM$_{2.5}$ derived from MAIAC AOD (**a**) and 3 km PM$_{2.5}$ derived from MODIS AOD (**c**) in Hubei Province in 2017. When the map is zoomed to a smaller scale, the spatial advantages of the 1 km PM$_{2.5}$ are displayed by comparing the MAIAC-derived (**b**) and MODIS-derived (**d**) PM$_{2.5}$ concentrations.

Additionally, MAIAC AOD with 1 km resolution could generate many more AOD-$PM_{2.5}$ pairs [52,53] than MODIS AOD with 3 km resolution. As a result, when the dataset becomes larger, the MAIAC AOD is able to reflect more information related to $PM_{2.5}$, and can achieve better results.

To evaluate the estimating accuracy, we extract the measured $PM_{2.5}$ values of ground monitoring site 1844A as the situ true values. The estimated $PM_{2.5}$ values are generated from MAIAC 1 km AOD and MODIS 3 km AOD. We analyzed the linear correlation of the measured and estimated $PM_{2.5}$ values, 0.6355 for MAIAC AOD and 0.5918 for MODIS AOD (shown as Figure 5). As the result shows, the $PM_{2.5}$ estimated from MAIAC AOD not only have higher spatial resolution, but also have higher estimating accuracy, which reveals the feasibility and superiority of MAIAC AOD in terms of $PM_{2.5}$ estimating.
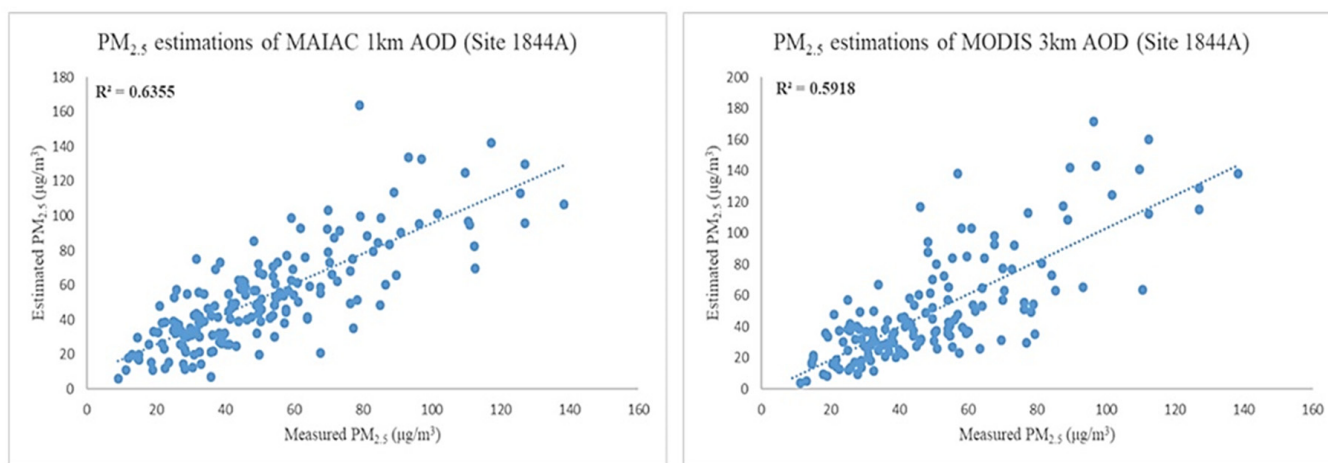

Figure 5. Linear Correlation Analysis of measured $PM_{2.5}$ and estimated $PM_{2.5}$, the estimated $PM_{2.5}$ are retrieved from MAIAC 1 km AOD and MODIS 3 km AOD.

3.2.2. Seasonal Pattern of the Estimated $PM_{2.5}$

To illustrate the temporal and seasonal pattern of $PM_{2.5}$ in the study area, the data for different seasons were extracted to construct the seasonal regression models and then estimate the $PM_{2.5}$ concentrations of different seasons. Figure 6 shows the seasonal mean value distributions of $PM_{2.5}$. Figure 6 shows that the $PM_{2.5}$ estimations derived from the optimal MSVR model using the 1 km resolution MAIAC AOD values as the model inputs had significant seasonal differences.

The $PM_{2.5}$ concentration values were generally low in summer, reaching the lowest values among the four seasons. Conversely, the $PM_{2.5}$ concentrations reached the highest level in winter, which might be the reason for more frequent air pollution weather in winter. In addition, the $PM_{2.5}$ concentrations in spring and autumn fell between the other two seasons, generally higher than summer and lower than winter, which could be explained by the seasonal climate differences.

The $PM_{2.5}$ concentration values were generally low in summer, reaching the lowest values among the four seasons. On the contrary, the $PM_{2.5}$ concentrations generally reached the high level in winter, which fitted the fact that the smoggy weather occurred more frequently in winter. Furthermore, from this side, our experiment results were reasonable. In addition, the $PM_{2.5}$ concentrations in spring and autumn fell between the other two seasons, generally higher than summer and lower than winter, which could be explained by the seasonal climate differences.
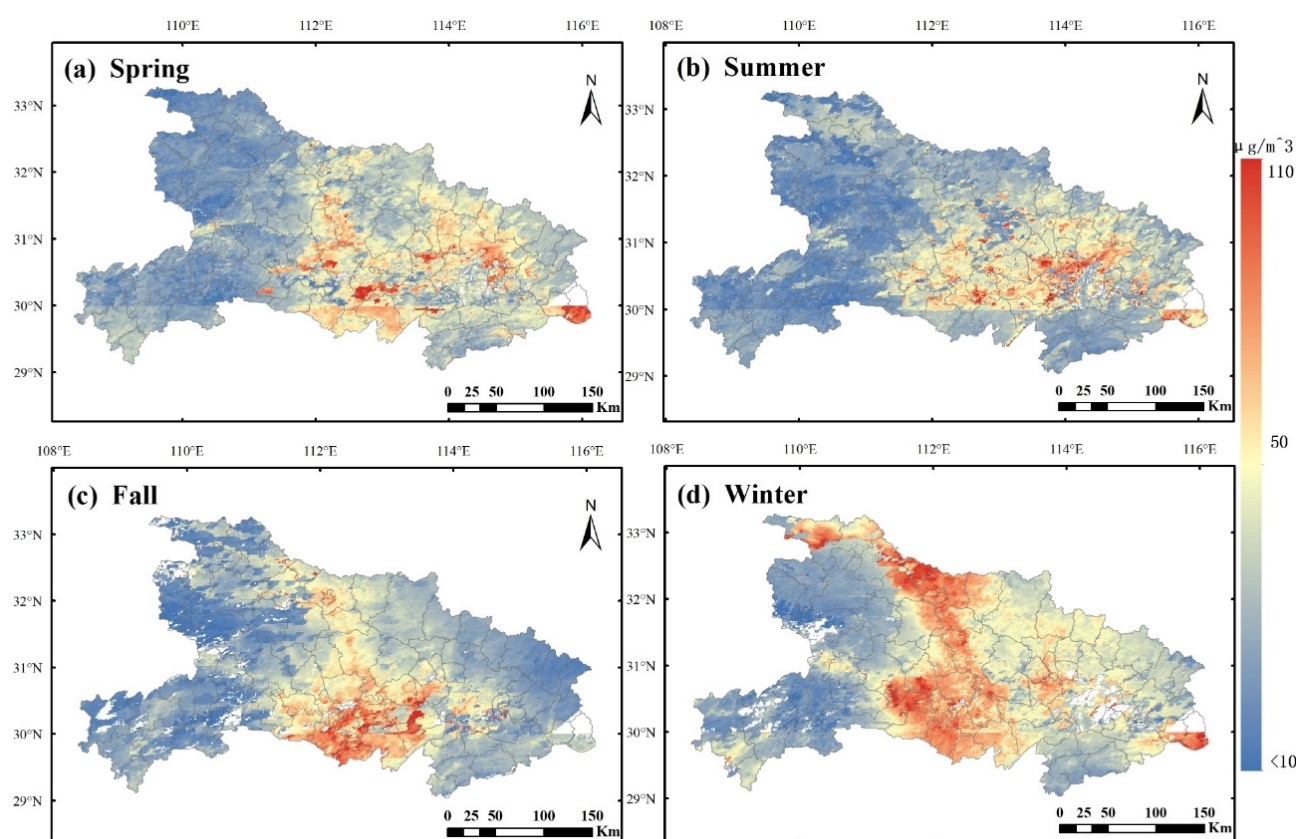
Figure 6. The distribution of and variation in averaged PM$_{2.5}$ estimations in four seasons (**a**) for spring, (**b**) for summer, (**c**) for autumn, and (**d**) for winter) in the study area of Hubei, China.

4. Discussion

4.1. Performance of the MSVR Model

Conventional Support Vector Regression (SVR) models were conducted on the same dataset to compare and evaluate the performance of MSVR. Three evaluation indexes, including the R^2, MPE and RMSE, were applied in the model performance evaluation. As recorded in Tables 4 and 5, the regression accuracy was influenced by season and model type and generally increased when models were established in different seasons (e.g., the summer model showed poor performance due to the absence of AOD data) compared to the whole year; additionally, the MSVR model generally had better performance than the SVR. The R^2 of the whole-year MSVR model increased by 0.14 compared to the SVR model, while the MPE and RMSE of the MSVR model decreased by 1.42 μg/m^3 and 1.73 μg/m^3, respectively. Considering the complexity of atmospheric retrieval and study area, surface reflectance impact, cloud contamination, etc., we think MSVR in this paper obtained relatively good performance.

The R^2, MPE and RMSE of the MSVR models generally increased in the four seasons, respectively. The measurements and estimation values at different scales for different seasons showed that the PM$_{2.5}$ concentration values changed over time. Generally, as the results illustrate, the PM$_{2.5}$ concentrations reached a peak value in winter and the lowest value in summer, which was in good agreement with existing empirical knowledge.

As shown in Figure 7, the estimated PM$_{2.5}$ and measured PM$_{2.5}$ are concentratedly distributed near the centerline, which means that the estimated PM$_{2.5}$ generally have the similar pattern with the measured PM$_{2.5}$ no matter for MSVR model or SVR model. According to the figure, most of PM$_{2.5}$ values fall between 20 μg/m^3 to 80 μg/m^3. And from the figure, the gap between the estimated and measured PM$_{2.5}$ values of SVR model

gets bigger when $PM_{2.5}$ values get higher. This means the MSVR model is more capable for accurate estimating in the high level of $PM_{2.5}$ values.

As the results showed, the MSVR model performed better than the conventional SVR model in $PM_{2.5}$ estimating. In addition, compared with other nonlinear models, such as the neural network, MSVR is more suitable for relatively small datasets, such as the dataset used in this paper. SVM has a solid mathematical theoretical basis and a strong generalization ability, which can effectively solve the problem of high-dimensional data model construction under limited sample size, and correspondingly, MSVR is relatively easy to construct and train compared to other nonlinear models.

Table 4. Accuracy comparisons between SVR and MSVR for different seasons and the entire year in 2017.

Model	Time Period	R^2	MPE ($\mu g/m^3$)	RMSE ($\mu g/m^3$)
SVR	Whole year (2017)	0.60	11.16	12.58
	Spring	0.61	12.14	14.53
	Summer	0.50	10.54	12.55
	Autumn	0.56	12.63	15.31
	Winter	0.64	13.35	15.68
Modified SVR (MSVR)	Whole year (2017)	0.74	9.74	10.85
	Spring	0.69	10.69	13.76
	Summer	0.53	8.33	10.36
	Autumn	0.70	10.01	14.02
	Winter	0.82	12.35	14.71

Table 5. Accuracy comparisons between SVR and MSVR for different seasons and the entire year in 2018.

Model	Time Period	R^2	MPE ($\mu g/m^3$)	RMSE ($\mu g/m^3$)
SVR	Whole year (2018)	0.66	10.11	12.85
	Spring	0.53	11.04	13.66
	Summer	0.52	9.62	11.47
	Autumn	0.60	11.39	13.18
	Winter	0.72	12.65	14.92
Modified SVR (MSVR)	Whole year (2018)	0.78	8.92	11.32
	Spring	0.61	9.58	11.89
	Summer	0.59	8.27	11.01
	Autumn	0.76	10.17	12.22
	Winter	0.80	11.64	12.15

4.2. Advantages of MAIAC AOD

In this paper, the MAIAC AOD with a spatial resolution of 1 km and the MODIS AOD with a spatial resolution of 3 km were utilized to estimate the ambient $PM_{2.5}$ concentrations with the same optimal model. According to the results, the $PM_{2.5}$ estimations from MAIAC AOD and MODIS AOD had similar spatial and temporal distributions. However, as shown in Figures 4 and 5, MAIAC AOD with 1 km resolution could generate many more AOD-$PM_{2.5}$ pairs than MODIS AOD with 3 km resolution. As a result, when the dataset becomes larger, the MAIAC AOD is able to reflect more information related to $PM_{2.5}$, and can achieve better results in the inversion. Researches have shown that the correlation between $PM_{2.5}$ and AOD decreased significantly as AOD resolution was degraded in spite of the intrinsic mismatch between $PM_{2.5}$ ground level measurements and AOD vertically integrated measurements [54]. This conclusion could also be seen from our analysis in Figure 5.

$PM_{2.5}$ retrievals of higher spatial resolution make it possible to figure out the spatial distribution characteristics. This is of great importance to accurately locate the source of air pollution where the $PM_{2.5}$ concentration usually abnormally elevates. Additionally, we

cannot ignore the other superiorities of MAIAC algorithm over the DB/DT algorithm. For example, high-resolution MAIAC is capable to distinguish aerosol sources and fine feature, MAIAC retrieval accuracy is higher than DT/DB with more accuracy over dark surface, and MAIAC has less sensitivity to variation in aerosol types across the seasons.
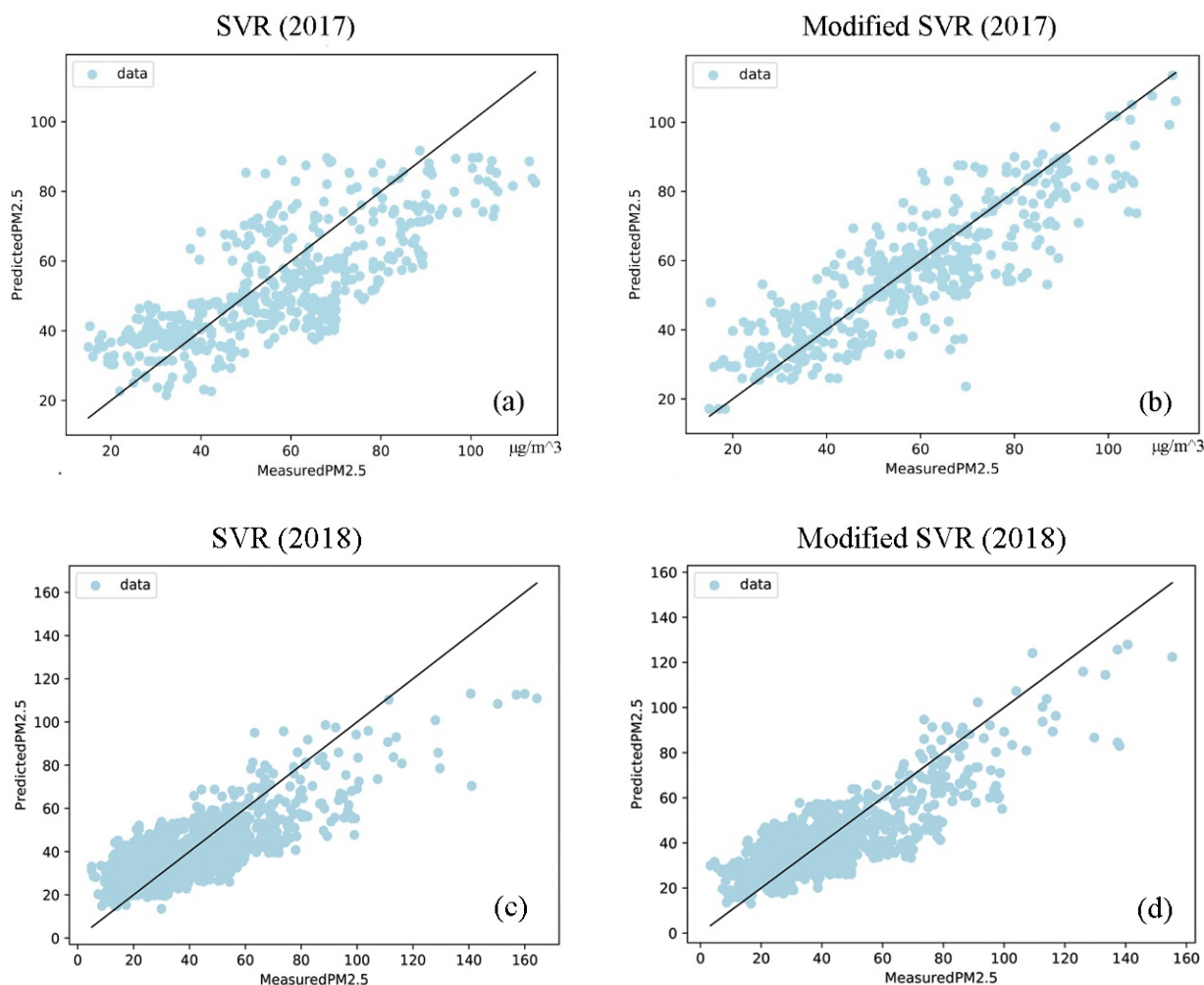

Figure 7. The scatterplots of cross validation results for SVR (**a**) and Modified SVR (**b**) models in 2017, SVR (**c**) and Modified Scheme 2018. (**d**) are shown in the figure. The horizontal axis represents the measured true PM$_{2.5}$ values and the vertical axis represents the predicted PM$_{2.5}$ obtained from the regression models. The black lines are the 1:1 reference line.

4.3. Analyses of the Spatiotemporal Pattern of PM$_{2.5}$

Firstly, as shown in Figure 3, it should be noted that most cities in the middle and southern parts, such as Jingzhou, Qianjiang, Jingmen, and Wuhan, have the higher PM$_{2.5}$ concentration level. This might be interpreted as the lager population, heavy vehicle emissions and more reliance on carbon-intensive industries for a significant proportion of their economic activities [55]. Additionally, researches show that secondary particles resulting from chemical reactions in primary gaseous pollutants may also contribute to levels in this region [51]. On the other hand, the lowest PM$_{2.5}$ level occurs in Shiyan, northwest of Hubei, with more mountainous woodland and vegetation cover and far lower anthropogenic emission levels, which is helpful for atmospheric dispersion and dilution.

Secondly, the PM$_{2.5}$ concentrations differ greatly across the seasons. The highest PM$_{2.5}$ levels in 2017 occurred during the winter and the lowest during the summer (Figure 6). Seasonal maximum PM$_{2.5}$ concentrations in winter may be the reason of coal combustion and unfavorable meteorological conditions for pollution dispersion in winter (such as the

stagnant weather and temperature inversion) [56]. It is worth noting that the secondary particles generated from chemical reactions in primary gaseous pollutants can contribute to fine PM formation. Summer was the season with the lowest average $PM_{2.5}$ concentration. This may be interpreted as the reduced anthropogenic emissions related to coal burning for domestic heating; summer monsoons can also help to dissipate aerosols [57].

4.4. Limitations

The MSVR method proposed in this paper has its own limitations. First, due to the missing AOD data on some days, which are usually caused by cloud cover and high surface reflectance, the number of AOD-$PM_{2.5}$ matchups per day is limited [58], resulting in model over-fitting or decreased estimation accuracy. Moreover, the focus of this experiment is the regression method. $PM_{2.5}$ feature analyses in large-scale and long period or in the urban areas are not detailed enough. In future work, more available satellite data with higher resolution and quality should be introduced into AOD-$PM_{2.5}$ research.

It is worth noting that MODIS AOD is a column average and not surface. There are satellite products that offer vertical profiles, and these are assimilated in MERRA-2 and ECMWF air chemistry sub-models, and could provide surface estimates [59]. However, in view of the current wide application of MODIS AOD and the current research on AOD of vertical profiles not being enough, we have not explored the impact of column average on the experiment. This is the focus of our future work.

In this experiment, we mainly added meteorological and land cover data but, in fact, the relationship between AOD and $PM_{2.5}$ is affected by many factors, such as the temperature inversion and more parameters including meteorological, topographic and society parameters [60]. The influence of these factors is relatively complex, and the current research is not yet mature. In future work, we will try to introduce more factors into the regression and analysis.

In addition, the composition and structure of atmospheric pollutants are quite complex and diverse [61], such as SO_2, NO_2, CO, O_3, etc. We will be committed in the research and retrieval of AOD and other more pollutants.

5. Conclusions

The satellite AOD data used in this experiment has superiority over the conventional DB/DT AOD in terms of resolution and accuracy. A higher resolution (1 km) satellite AOD data is used to ensure that the obtained $PM_{2.5}$ can reflect more accurate and detailed temporal and spatial characteristics. Additionally, the accuracy of MAIAC algorithm has been proved to be higher than DT/DB algorithm over dark surface. The experiment verified the feasibility of 1 km MAIAC AOD for $PM_{2.5}$ retrieval and the superiority over the 3 km MODIS AOD in terms of spatial resolution and retrieval accuracy.

MSVR proposed in this paper, is modified based on the traditional SVR for the regression of AOD and $PM_{2.5}$ and obtain the improvement of experiment accuracy. The results showed that the MSVR model could improve the accuracy of the regression from R^2 0.60 to 0.74 in 2017 and 0.66 to 0.78 in 2018 compared to the traditional SVR.

We introduced the commonly used meteorological parameters to reduce the influence of complex factors on $PM_{2.5}$ retrieval from satellite AOD to a certain extent. The integrated meteorological parameters and land cover data demonstrated that the appropriate auxiliary variables could improve the performance of $PM_{2.5}$ retrieval.

The experimental results also showed that $PM_{2.5}$ has obvious spatial and temporal differences. We analyzed the spatial and temporal distribution and characteristics of $PM_{2.5}$ in Hubei Province, and conducted the above analysis by season. We also analyzed the possible reason of such spatiotemporal differences.

In our future work, we will make efforts from three aspects. First, we will try to find satellites with higher resolution and aerosol retrieval algorithm with better performance. It is worth noting that, recently, there are studies that propose combining satellite remote-sensing techniques and a newly established low-cost sensor network to estimate long-

term PM$_{2.5}$ concentrations to increase the measurement density. Secondly, we will try to figure out the specific influence of meteorological, topographic and social factors on the distribution characteristics of PM$_{2.5}$ and the retrieval of PM$_{2.5}$ from satellite AOD. Thirdly, we will attempt to conduct longer time series and wider range of analyses of PM$_{2.5}$ distribution characteristics.

Conflicts of Interest: We declare that we have no financial and personal relationships with other people or organizations that can inappropriately influence our work, there is no professional or other personal interest of any nature or kind in any product, service and/or company that could be construed as influencing the position presented in, or the review of, the manuscript entitled.

References

1. Landrigan, P.J.; Fuller, R.; Acosta, N.J.R.; Adeyi, O.; Arnold, R.; Basu, N.; Baldé, A.B.; Bertollini, R.; Bose-O'Reilly, S.; Boufford, J.I.; et al. The Lancet Commission on pollution and health. *Lancet* **2018**, *391*, 462–512. [CrossRef]
2. Beelen, R.; Raaschou-Nielsen, O.; Stafoggia, M.; Andersen, Z.J.; Weinmayr, G.; Hoffmann, B.; Wolf, K.; Samoli, E.; Fischer, P.; Nieuwenhuijsen, M.J.; et al. Effects of long-term exposure to air pollution on natural-cause mortality: An analysis of 22 European cohorts within the multicentre ESCAPE project. *Lancet* **2014**, *383*, 785–795. [CrossRef]
3. Polezer, G.; Tadano, Y.S.; Siqueira, H.V.; Godoi, A.F.; Yamamoto, C.I.; De André, P.A.; Pauliquevis, T.; Andrade, M.D.F.; Oliveira, A.; Saldiva, P.H.; et al. Assessing the impact of PM2.5 on respiratory disease using artificial neural networks. *Environ. Pollut.* **2018**, *235*, 394–403. [CrossRef] [PubMed]
4. Chan, Y.C.; Simpson, R.W.; Mctainsh, G.H.; Vowles, P.D.; Cohen, D.D. Characterisation of chemical species in PM2.5 and PM10 aerosols in Brisbane, Australia. *Atmos. Environ.* **2015**, *37*, 31–39. [CrossRef]
5. Wang, Y.; Jia, C.; Tao, H.; Zhang, L.; Liang, X.; Ma, J.-M.; Gao, H.; Huang, T.; Zhang, K. Chemical characterization and source apportionment of PM2.5 in a semi-arid and petrochemical-industrialized city, Northwest China. *Sci. Total Environ.* **2016**, *573*, 1031–1040. [CrossRef] [PubMed]
6. Ma, Z.; Hu, X.; Sayer, A.M.; Levy, R.; Zhang, Q.; Xue, Y.; Tong, S.; Bi, J.; Huang, L.; Liu, Y. Satellite-based spatiotem-poral trends in PM2. 5 concentrations: China. *Environ. Health Perspect.* **2016**, *124*, 184–192. [CrossRef] [PubMed]
7. Li, S.; Joseph, E.; Min, Q. Remote sensing of ground-level PM2.5 combining AOD and backscattering profile. *Remote Sens. Environ.* **2016**, *183*, 120–128. [CrossRef]
8. Paciorek, C.J.; Yang, L. AOD–PM2.5 Association: Paciorek and Liu Respond. *Environ. Health Perspect.* **2010**, *118*, A110–A111. [CrossRef]
9. Zhang, T.; Gong, W.; Wang, W.; Ji, Y.; Zhu, Z.; Huang, Y. Ground Level PM2.5 Estimates over China Using Satellite-Based Geographically Weighted Regression (GWR) Models Are Improved by Including NOâ,, and Enhanced Vegetation Index (EVI). *Int. J. Environ. Res. Public Health* **2016**, *13*, 1215. [CrossRef]
10. Wei, J.; Huang, W.; Li, Z.; Xue, W.; Peng, Y.; Sun, L.; Cribb, M. Estimating 1-km-resolution PM2.5 concentrations across China using the space-time random forest approach. *Remote Sens. Environ.* **2019**, *231*, 111221. [CrossRef]
11. Xia, X.; Qi, Q.; Liang, H.; Zhang, A.; Jiang, L.; Ye, Y.; Liu, C.; Huang, Y. Pattern of spatial distribution and tem-poral variation of atmospheric pollutants during 2013 in Shenzhen, China. *ISPRS Int. J. Geoinf.* **2017**, *6*, 2. [CrossRef]

12. Gross, B.; Schäfer, K.; Keckhut, P. Special Section Guest Editorial: Advances in Remote Sensing for Air Quality Management. *J. Appl. Remote Sens.* **2018**, *12*, 042601. [CrossRef]

13. Park, S.; Choi, J. Satellite-measured atmospheric aerosol content in Korea: Anthropogenic signals from decadal records. *GISci. Remote Sens.* **2016**, *53*, 1–17. [CrossRef]

14. Yuanyu, X.; Yuxuan, W.; Kai, Z.; Wenhao, D.; Baolei, L.; Yuqi, B. Daily Estimation of Ground-Level PM2.5 Concentrations over Beijing Using 3 km Resolution MODIS AOD. *Environ. Sci. Technol.* **2015**, *49*, 12280–12288.

15. You, W.; Zang, Z.; Zhang, L.; Li, Y.; Wang, W. Estimating national-scale ground-level PM25 concentration in China using geographically weighted regression based on MODIS and MISR AOD. *Environ. Sci. Pollut. Res.* **2016**, *23*, 8327–8338. [CrossRef]

16. You, W.; Zang, Z.; Pan, X.; Zhang, L.; Chen, D. Estimating PM2.5 in Xi'an, China using aerosol optical depth: A comparison between the MODIS and MISR retrieval models. *Sci. Total. Environ.* **2015**, *505*, 1156–1165. [CrossRef]

17. Zang, L.; Mao, F.; Guo, J.; Gong, W.; Wang, W.; Pan, Z. Estimating hourly PM1 concentrations from Himawari-8 aerosol optical depth in China. *Environ. Pollut.* **2018**, *241*, 654–663. [CrossRef]

18. Yumimoto, K.; Nagao, T.M.; Kikuchi, M.; Sekiyama, T.T.; Murakami, H.; Tanaka, T.Y.; Ogi, A.; Irie, H.; Khatri, P.; Okumura, H. Aerosol data assimilation using data from Himawari-8, a next-generation geostationary meteorological satellite: Aero-sol assimilation with Himawari-8. *Geophys. Res. Lett.* **2016**, *43*, 5886–5894. [CrossRef]

19. Yao, F.; Si, M.; Li, W.; Wu, J. A multidimensional comparison between MODIS and VIIRS AOD in estimating ground-level PM2.5 concentrations over a heavily polluted region in China. *Sci. Total Environ.* **2018**, *618*, 819–828. [CrossRef]

20. Mhawish, A.; Banerjee, T.; Sorek-Hamer, M.; Lyapustin, A.; Broday, D.M.; Chatfield, R. Comparison and evaluation of MODIS Multi-angle Implementation of Atmospheric Correction (MAIAC) aerosol product over South Asia. *Remote Sens. Environ.* **2019**, *224*, 12–28. [CrossRef]

21. Lyapustin, A.; Wang, Y.; Korkin, S.; Huang, D. MODIS Collection 6 MAIAC algorithm. *Atmos. Meas. Tech.* **2018**, *11*, 5741–5765. [CrossRef]

22. Boyouk, N.; Léon, J.-F.; Delbarre, H.; Podvin, T.; DeRoo, C. Impact of the mixing boundary layer on the relationship between PM2.5 and aerosol optical thickness. *Atmos. Environ.* **2010**, *44*, 271–277. [CrossRef]

23. Zheng, C.; Zhao, C.; Zhu, Y.; Wang, Y.; Shi, X.; Wu, X.; Chen, T.; Wu, F.; Qiu, Y. Analysis of influential factors for the relationship between PM2.5 and AOD in Beijing. *Atmos. Chem. Phys. Discuss.* **2017**, *17*, 13473–13489. [CrossRef]

24. Ma, Z.; Hu, X.; Huang, L.; Bi, J.; Liu, Y. Estimating Ground-Level PM2.5 in China Using Satellite Remote Sensing. *Environ. Sci. Technol.* **2014**, *48*, 7436–7444. [CrossRef] [PubMed]

25. Guo, J.; Xia, F.; Zhang, Y.; Liu, H.; Li, J.; Lou, M.; He, J.; Yan, Y.; Wang, F.; Min, M.; et al. Impact of diurnal variability and meteorological factors on the PM2.5—AOD relationship: Implications for PM2.5 remote sensing. *Environ. Pollut.* **2017**, *221*, 94–104. [CrossRef]

26. Liu, Y.; Paciorek, C.J.; Koutrakis, P. Estimating Regional Spatial and Temporal Variability of PM 2.5 Concentrations Using Satellite Data, Meteorology, and Land Use Information. *Environ. Health Perspect.* **2009**, *117*, 886–892. [CrossRef]

27. Xiao, L.; Lang, Y.; Christakos, G.J.A.E. High-resolution spatiotemporal mapping of PM2. 5 concentrations at Mainland Chi-na using a combined BME-GWR technique. *Atmos. Environ.* **2018**, *173*, 295–305. [CrossRef]

28. Zhai, L.; Li, S.; Zou, B.; Sang, H.; Fang, X.; Xu, S. An improved geographically weighted regression model for PM 2.5 concentration estimation in large areas. *Atmos. Environ.* **2018**, *181*, 145–154. [CrossRef]

29. Su, T.; Li, J.; Li, C.; Lau, A.K.-H.; Yang, D.; Shen, C. An intercomparison of AOD-converted PM2.5 concentrations using different approaches for estimating aerosol vertical distribution. *Atmos. Environ.* **2017**, *166*, 531–542. [CrossRef]

30. Chen, G.; Li, S.; Knibbs, L.D.; Hamm, N.; Cao, W.; Li, T.; Guo, J.; Ren, H.; Abramson, M.J.; Guo, Y. A machine learning method to estimate PM2.5 concentrations across China with remote sensing, meteorological and land use information. *Sci. Total Environ.* **2018**, *636*, 52–60. [CrossRef]

31. Yang, Q.; Yuan, Q.; Yue, L.; Li, T.; Shen, H.; Zhang, L. The relationships between PM2.5 and aerosol optical depth (AOD) in mainland China: About and behind the spatio-temporal variations. *Environ. Pollut.* **2019**, *248*, 526–535. [CrossRef] [PubMed]

32. Yang, W.; Deng, M.; Xu, F.; Wang, H. Prediction of hourly PM2.5 using a space-time support vector regression model. *Atmos. Environ.* **2018**, *181*, 12–19. [CrossRef]

33. Roy, A.; Chakraborty, S. Support vector regression based metamodel by sequential adaptive sampling for reliability analysis of structures. *Reliab. Eng. Syst. Saf.* **2020**, *200*, 106948. [CrossRef]

34. Zhang, T.; Zhu, Z.; Gong, W.; Zhu, Z.; Sun, K.; Wang, L.; Huang, Y.; Mao, F.; Shen, H.; Li, Z.; et al. Estimation of ultrahigh resolution PM2.5 concentrations in urban areas using 160 m Gaofen-1 AOD retrievals. *Remote Sens. Environ.* **2018**, *216*, 91–104. [CrossRef]

35. Giles, D.M.; Sinyuk, A.; Sorokin, M.G.; Schafer, J.S.; Smirnov, A.; Slutsker, I.; Eck, T.F.; Holben, B.N.; Lewis, J.R.; Campbell, J.R. Advancements in the Aerosol Robotic Network (AERONET) Version 3 database–automated near-real-time quality control algorithm with improved cloud screening for Sun photometer aerosol optical depth (AOD) measurements. *Atmos. Meas. Tech.* **2019**, *12*, 169–209. [CrossRef]

36. Zhang, Z.; Wu, W.; Fan, M.; Wei, J.; Tan, Y.; Wang, Q. Evaluation of MAIAC aerosol retrievals over China. *Atmos. Environ.* **2019**, *202*, 8–16. [CrossRef]

37. Chen, G.; Knibbs, L.D.; Zhang, W.; Li, S.; Cao, W.; Guo, J.; Ren, H.; Wang, B.; Wang, H.; Williams, G. Estimating spatiotem-poral distribution of PM1 concentrations in China with satellite remote sensing, meteorology, and land use information. *Environ. Pollut.* **2018**, *233*, 1086–1094. [CrossRef]

38. Wang, J.; Ogawa, S. Effects of Meteorological Conditions on PM2.5 Concentrations in Nagasaki, Japan. *Int. J. Environ. Res. Public Health* **2015**, *12*, 9089–9101. [CrossRef]

39. Huang, F.; Xia, L.; Chao, W.; Qin, X.; Wei, W.; Luo, Y.; Tao, L.; Qi, G.; Jin, G.; Chen, S.; et al. PM2.5 Spatiotemporal Variations and the Relationship with Meteorological Factors during 2013-2014 in Beijing, China. *PLoS ONE* **2015**, *10*, e0141642. [CrossRef]

40. Trifonova, T.A.; Mishchenko, N.V.; Grishina, Y.P. A remote sensing-based method for determining industrial air pollution. *Mapp. Sci. Remote Sens.* **1998**, *35*, 22–30. [CrossRef]

41. Chen, B.; Li, S.; Yang, X.; Lu, S.; Wang, B.; Niu, X. Characteristics of atmospheric PM2.5 in stands and non-forest cover sites across urban-rural areas in Beijing, China. *Urban Ecosyst.* **2016**, *19*, 867–883. [CrossRef]

42. Kumar, A. Long term (2003–2012) spatiotemporal MODIS (Terra/Aqua level 3) derived climatic variations of aerosol opti-cal depth and cloud properties over a semiarid urban tropical region of Northern India. *Atmos. Environ.* **2014**, *83*, 291–300. [CrossRef]

43. Hao, Y.; Liu, Y. The influential factors of urban PM2.5 concentrations in China: A spatial econometric analysis. *J. Clean. Prod.* **2016**, *112*, 1443–1453. [CrossRef]

44. Kelly, K.M.; Dennis, M.L. Transforming between WGS84 Realizations and other Reference Frames. In *AGU Fall Meeting Abstracts*; American Geophysical Union: Washington, DC, USA, 2018.

45. Noble, W. What is a support vector machine? *Nat. Biotechnol.* **2006**, *24*, 1565–1567. [CrossRef] [PubMed]

46. Smola, A.J.; Schölkopf, B. A tutorial on support vector regression. *Stat. Comput.* **2004**, *14*, 199–222. [CrossRef]

47. Chang, C.-C.; Lin, C.-J. LIBSVM: A library for support vector machines. *ACM Trans. Intell. Syst. Technol.* **2011**, *2*, 27. [CrossRef]

48. Zhu, S.; Lian, X.; Wei, L.; Che, J.; Shen, X.; Yang, L.; Qiu, X.; Liu, X.; Gao, W.; Ren, X.; et al. PM2.5 forecasting using SVR with PSOGSA algorithm based on CEEMD, GRNN and GCA considering meteorological factors. *Atmos. Environ.* **2018**, *183*, 20–32. [CrossRef]

49. Awad, M.; Khanna, R. Support vector regression. In *Efficient Learning Machines*; Apress: Berkeley, CA, USA, 2015; pp. 67–80.

50. Wang, S.; Zhou, C.; Wang, Z.; Feng, K.; Hubacek, K. The characteristics and drivers of fine particulate matter (PM2.5) distribution in China. *J. Clean. Prod.* **2017**, *142*, 1800–1809. [CrossRef]

51. Balasundaram, S. On Lagrangian support vector regression. *Expert Syst. Appl.* **2010**, *37*, 8784–8792. [CrossRef]

52. Chudnovsky, A.; Tang, C.; Lyapustin, A.; Wang, Y.; Schwartz, J.; Koutrakis, P.J.A.C. A critical assessment of high-resolution aerosol optical depth retrievals for fine particulate matter predictions. *Atmos. Chem. Phys.* **2013**, *13*, 10907. [CrossRef]

53. Chudnovsky, A.A.; Koutrakis, P.; Kloog, I.; Melly, S.J.; Nordio, F.; Lyapustin, A.I.; Wang, Y.; Schwartz, J. Fine particulate matter predictions using high resolution Aerosol Optical Depth (AOD) retrievals. *Atmos. Environ.* **2014**, *89*, 189–198. [CrossRef]

54. Chudnovsky, A.A.; Kostinski, A.; Lyapustin, A.; Koutrakis, P.J.E.P. Spatial scales of pollution from variable resolution satellite imaging. *Environ. Pollut.* **2013**, *172*, 131–138. [CrossRef] [PubMed]

55. Guan, D.; Su, X.; Zhang, Q.; Peters, G.P.; Liu, Z.; Lei, Y.; He, K. The socioeconomic drivers of China's primary PM 2.5 emissions. *Environ. Res. Lett.* **2014**, *9*, 024010. [CrossRef]

56. Huang, T.; Yu, Y.; Wei, Y.; Wang, H.; Huang, W.; Chen, X. Spatial–seasonal characteristics and critical impact factors of PM2. 5 concentration in the Beijing–Tianjin–Hebei urban agglomeration. *PLoS ONE* **2018**, *13*, e0201364.

57. Cheng, Z.; Li, L.; Liu, J. Identifying the spatial effects and driving factors of urban PM2.5 pollution in China. *Ecol. Indic.* **2017**, *82*, 61–75. [CrossRef]

58. Lin, C.; Labzovskii, L.; Mak, H.W.L.; Fung, J.C.; Lau, A.K.; Kenea, S.T.; Bilal, M.; Hey, J.D.V.; Lu, X.; Ma, J. Observation of PM2.5 using a combination of satellite remote sensing and low-cost sensor network in Siberian urban areas with limited reference monitoring. *Atmos. Environ.* **2020**, *227*, 117410. [CrossRef]

59. Toth, T.D.; Zhang, J.; Campbell, J.R.; Hyer, E.; Reid, J.S.; Shi, Y.; Westphal, D.L. Impact of data quality and surface-to-column representativeness on the PM2.5/satellite AOD relationship for the contiguous United States. *Atmos. Chem. Phys. Discuss.* **2014**, *14*, 6049–6062. [CrossRef]

60. Zang, Z.; Wang, W.; You, W.; Li, Y.; Ye, F.; Wang, C. Estimating ground-level PM2.5 concentrations in Beijing, China using aerosol optical depth and parameters of the temperature inversion layer. *Sci. Total. Environ.* **2017**, *575*, 1219–1227. [CrossRef]

61. Lalitaporn, P.; Kurata, G.; Matsuoka, Y.; Thongboonchoo, N.; Surapipith, V.J. Long-term analysis of no 2, co, and aod seasonal variability using satellite observations over asia and intercomparison with emission inventories and model. *Atmos. Health* **2013**, *6*, 655–672. [CrossRef]